

A new diagnostic for the null test of dynamical dark energy in light of DESI 2024 and other BAO data

Bikash R. Dinda ^{a,1}

^aDepartment of Physics & Astronomy, University of the Western Cape, Cape Town, 7535, South Africa.

E-mail: bikashd18@gmail.com

Abstract. We introduce a new diagnostic for the null test of dynamical dark energy. This diagnostic is useful, especially when we include anisotropic baryon acoustic oscillation (BAO) data in an analysis, to quantify the deviations from the standard Λ CDM model. This null test is independent of any late-time cosmological model or parametrization. With this, we study the evidence for dynamical dark energy in light of Dark Energy Spectroscopic Instrument (DESI) 2024 data combined with cosmic microwave background (CMB) observations of the Planck 2018 mission and local H_0 measurements. We find low (around 0.6σ) to moderate (around 1σ) evidence for dynamical dark energy which is not that significant. Although we get individual deviations at around 2σ at the effective redshift 0.51 of the DESI 2024 data, the average deviations combining all redshift points are almost independent of the inclusion or exclusion of the data at effective redshift 0.51 (the differences are only around 0.3σ). We get almost similar results for other non-DESI BAO data. The evidences are almost independent of the early-time physics and these evidences have very low dependence on H_0 values. The evidence of dynamical dark energy, obtained in this analysis, is not consistent with the DESI key paper results with the w_0w_a CDM model, but interestingly, these are almost consistent with the DESI's results with z_pw_p CDM model.

¹Corresponding author.

Contents

1	Introduction	1
2	The new diagnostic	3
3	Observational data	6
3.1	DESI 2024 BAO	6
3.2	Planck CMB mission 2018: CMB distance priors	6
3.3	H_0 measurements	8
3.4	Other BAO data	8
4	Results	10
5	Conclusion	14
A	Analytical expression of comoving distance in ΛCDM model	18
B	Computation of A and ΔA corresponding to DESI 2024 and other BAO data	20
C	Approximate sound horizon at the early time with standard early time physics	22
D	Approximate redshift of photon decoupling with standard early time physics	25
E	Brief overview of wCDM, w_0w_aCDM, and z_pw_pCDM parametrizations	25

1 Introduction

Ever since the discovery of the late time cosmic acceleration from the type Ia supernova observations [1–4], this phenomenon has been confirmed by several other observations such as cosmic microwave background (CMB) observations [5–7], baryon acoustic oscillation (BAO) observations [8–10], and cosmic chronometers (CC) observations for the Hubble parameter [11–13] etc.

Arguably, the most accepted explanation for the late time cosmic acceleration is the introduction of an exotic matter, called dark energy, as a possible constituent of the Universe and most importantly the dominant one in the late time era. Unlike any other matter, due to the large negative pressure of the dark energy, it has an effective repulsive gravity which in turn causes the late time cosmic acceleration of the Universe [14–21].

Since the introduction of the concept of dark energy, model building and phenomenological studies of the nature of dark energy have become crucial for understanding the evolutionary history of the Universe. Regarding this, the most popular model of dark energy is the Λ CDM model. In this model, a cosmological constant Λ is considered to be the candidate for the dark energy and the equation of state of this Λ is -1 which causes the late time expansion of the Universe to be accelerating [22].

The Λ CDM model stood out to be the most successful model to explain the majority of the cosmological observations, mentioned above. This is the reason it became the most popular model for the evolution of the Universe. It is sometimes called the standard model of cosmology (with the inclusion of inflation at a very early time era). Despite its huge success, there are some serious issues with this model. For example, theoretically, this model possesses the fine-tuning and cosmic coincidence problems [23–26]. From the observational point of view, there are issues like the Hubble tension [27–30], in which there is discrepancy in the observed values of the Hubble parameter between the early time (e.g. CMB [7]) and the late time (e.g. SHOES [31]) observations.

Because of these shortcomings of the Λ CDM model, it is thus important to consider dynamical dark energy models to study the nature of the dark energy and to check evidence of these alternative models in light of recent and upcoming observations. Note that, in the Λ CDM model, the energy density of the dark energy is constant in cosmic time. Hence, any model with evolving energy density of the dark energy is considered to be the dynamical dark energy models such as quintessence [32], k-essence [33], and Chevallier-Polarski-Linder (CPL) [34, 35] models.

Recently, the Dark Energy Spectroscopic Instrument (DESI) 2024 Data Release 1 (DR1) BAO observations (with and without the addition of CMB [7] and type Ia supernova observations [36–38] both separately and jointly) have found more than 2σ evidence for the dynamical dark energy considering the CPL model (most commonly known as the w_0w_a CDM model) [39]. Similar results with similar data are presented in a different analysis in Wang (2024) [40]. Interestingly, with the w_0w_a CDM model, similar kind of evidence for dynamical dark energy has been reported with other BAO data in Park et al. (2024) [41]. Besides these, the DESI 2024 data along with other data like CMB and the type Ia supernova have been considered to constrain different model parameters in different models [42–52]. Also, note that the Λ CDM model has been revisited with the DESI 2024 data in a different approach through the estimation of the present value of matter energy density parameter in Colg ain et al. (2024) [53].

Another interesting fact is that the same DESI 2024 data (with or without the same other data, mentioned earlier) shows that there is no evidence for dynamical dark energy when considering the w CDM model. Note that, while both w CDM and w_0w_a CDM models correspond to the dynamical dark energy, the equation of state of dark energy is constant in the w CDM model but evolving in w_0w_a CDM model. In another DESI paper by Calderon et al. (2024) [54], evidence for dynamical dark energy has been studied through crossing statistics and the results are different between crossing statistics applied to equation of state and the (normalized) energy density of dark energy (compare figures 1 and 3 in Calderon et al. (2024) [54]). In another study, with similar data, Luongo & Muccino (2024) [55] has reported that the w CDM model is favored over the CPL model through a model-independent cosmographic approach. Thus, the evidence for dynamical dark energy may be biased depending on different models [56]. Also, the priors on the dark energy parameters (see Cort es & Liddle (2024) [57]) and the degeneracies (see Shlivko & Steinhardt (2024) [58]) may affect the evidence if we consider a particular dark energy model or parametrization. Thus, in this regard, any model-independent (and for the betterment non-parametric too) approach will be useful to firmly test the evidence for dynamical dark energy.

In this study, we perform a model-independent null test of the evidence for dynamical dark energy by introducing a new diagnostic approach to study the deviation from the standard Λ CDM model. Because this approach is model-independent, there is no issue of bias

in the results. Also, the results are independent of any priors on the dark energy parameters, since there are no such parameters involved in this null test. Thus, this kind of null test is crucial for the evidence of dynamical dark energy. This new diagnostic is more useful compared to other existing diagnostics like the Om diagnostic [59, 60], particularly when we consider BAO observations because this diagnostic takes into account both the parallel and perpendicular anisotropic BAO measurements to the line of sight at the same time. Also, this new diagnostic is independent of the sound horizon at the baryon drag epoch, the parameter involved in the BAO measurements.

This paper is organized as follows: In Sec. 2, we introduce a new diagnostic for the null test of dynamical dark energy; in Sec. 3, we briefly discuss different cosmological data, considered in this analysis, including the recent DESI 2024 data; in Sec. 4, we present the results for the evidence of dynamical dark energy corresponding to different data combinations; and finally, we conclude this study in Sec. 5. We have also included some relevant details in the appendices. In Appendix A, we have provided the derivation for the analytical expression of the comoving distance as a function of redshift for the Λ CDM model. In Appendix B, we have discussed the DESI 2024 and other BAO data in detail and compared those. In Appendix C, we have provided an analytical approximate expression for the sound horizon applicable at higher redshift with the standard early-time cosmological physics and in Appendix D, we have provided a corresponding approximate expression of the redshift of photon decoupling. In Appendix E, we have briefly discussed the w CDM, the w_0w_a CDM, and the z_pw_p CDM parametrizations.

2 The new diagnostic

We consider flat Friedmann-Lemaître-Robertson-Walker (FLRW) metric for the background evolution of the Universe. For this case, the transverse comoving distance D_M is the same as the line of sight comoving distance and it is defined as [61]

$$D_M(z) = \frac{c}{H_0} \int_0^z \frac{d\tilde{z}}{E(\tilde{z})}, \quad (2.1)$$

where z (also \tilde{z}) is the redshift, c is the speed of light in vacuum, H_0 is the present value of the Hubble parameter, and E is the normalized Hubble parameter.

For a flat Λ CDM model, for the late-time evolution, the normalized Hubble parameter (denoted as $E_{\Lambda\text{CDM}}^{\text{late-time}}$) is given as

$$E_{\Lambda\text{CDM}}^{\text{late-time}}(z) = \sqrt{\Omega_{m0}(1+z)^3 + 1 - \Omega_{m0}}, \quad (2.2)$$

where Ω_{m0} is the present value of the matter energy density parameter. In Eq. (2.2), we have neglected the contribution from the radiation counterpart because we are using this equation for the late-time evolution only.

Putting Eq. (2.2) in Eq. (2.1), and performing the integration analytically, we get a corresponding expression for the comoving distance given as [30]

$$D_{M \Lambda\text{CDM}}^{\text{late-time}}(z) = \frac{c}{H_0 \sqrt{1 - \Omega_{m0}}} \left[(1+z) {}_2F_1 \left(\frac{1}{3}, \frac{1}{2}; \frac{4}{3}; -\frac{\Omega_{m0}(1+z)^3}{1 - \Omega_{m0}} \right) - {}_2F_1 \left(\frac{1}{3}, \frac{1}{2}; \frac{4}{3}; -\frac{\Omega_{m0}}{1 - \Omega_{m0}} \right) \right], \quad (2.3)$$

where ${}_2F_1$ represents the standard hypergeometric function. We have included the derivation of $D_{\text{M}\Lambda\text{CDM}}^{\text{late-time}}$ in Appendix A.

A quantity D_H is used in the baryon acoustic oscillations (BAO) observations defined as

$$D_H(z) = \frac{c}{H(z)} = \frac{c}{H_0 E(z)}, \quad (2.4)$$

where H is the Hubble parameter. Putting Eq. (2.2) in Eq. (2.4), we get the corresponding expression for D_H for the ΛCDM model at late times given as

$$D_{\text{H}\Lambda\text{CDM}}^{\text{late-time}}(z) = \frac{c}{H_0 \sqrt{\Omega_{\text{m}0}(1+z)^3 + 1 - \Omega_{\text{m}0}}}. \quad (2.5)$$

We define a quantity A given as [39, 53, 62]

$$A(z) = \frac{D_M(z)}{z D_H(z)}. \quad (2.6)$$

The reason to define the quantity A in this way is as follows. The BAO observations provide data of $\frac{D_M}{r_d}$ and $\frac{D_H}{r_d}$, but not directly D_M and D_H . Here r_d is the sound horizon at the baryon drag epoch. So, when we divide D_M by D_H , the ratio becomes independent of r_d . In general case, we get the expression of A , by putting Eqs. (2.1) and (2.4) in Eq. (2.6), given as

$$A(z) = \frac{D_M(z)}{z D_H(z)} = \frac{\frac{D_M(z)}{r_d}}{z \frac{D_H(z)}{r_d}} = \frac{E(z)}{z} \int_0^z \frac{d\tilde{z}}{E(\tilde{z})}. \quad (2.7)$$

Interestingly, in the above equation, we can see that, A can be computed only if we know the evolution of E . The evolution of E can be known from any cosmological model, but here, in this analysis, we do not consider any cosmological model, rather we will compute $A(z)$ directly from the BAO data using the second equality in the expression of A in Eq. (2.7). The reason and the purpose of this is that we are not doing any parameter estimation using any model. This is eventually discussed and will be clarified in the later parts. The redshift z in the denominator in the definition of A in Eq. (2.6) (or in the expression of A in Eq. (2.7)) is introduced to make it consistent to compare with the DESI 2024 paper results (see top-right panel of figure 1 in Adame et al. (2024) (DESI Collaboration) [39]).

Note that, there is no issue of infinity when we use the definition of A in Eq. (2.6) (or in Eq. (2.7)) at $z = 0$ due to the presence of z in the denominator. This is because, in the $z \rightarrow 0$ limit, A tends to 1. Anyway, we do not need to compute the value of A at $z = 0$, because there is no data at $z = 0$ (at least in our analysis).

Putting Eqs. (2.3) and (2.5) in Eq. (2.6) (or in Eq. (2.7)), we get the corresponding expression for A for the ΛCDM model at late times given as

$$A_{\Lambda\text{CDM}}^{\text{late-time}}(z) = \frac{\sqrt{\Omega_{\text{m}0}(1+z)^3 + 1 - \Omega_{\text{m}0}}}{z \sqrt{1 - \Omega_{\text{m}0}}} \times \left[(1+z) {}_2F_1 \left(\frac{1}{3}, \frac{1}{2}; \frac{4}{3}; -\frac{\Omega_{\text{m}0}(1+z)^3}{1 - \Omega_{\text{m}0}} \right) - {}_2F_1 \left(\frac{1}{3}, \frac{1}{2}; \frac{4}{3}; -\frac{\Omega_{\text{m}0}}{1 - \Omega_{\text{m}0}} \right) \right]. \quad (2.8)$$

We now define a quantity B given as $B(z) = \frac{A(z)}{A_{\Lambda\text{CDM}}^{\text{late-time}}(z)}$ and using Eq. (2.8), we get expression of B given as

$$B(z) = \frac{z\sqrt{1-\Omega_{m0}} A(z)}{\sqrt{\Omega_{m0}(1+z)^3 + 1 - \Omega_{m0}}} \times \left[(1+z) {}_2F_1\left(\frac{1}{3}, \frac{1}{2}; \frac{4}{3}; -\frac{\Omega_{m0}(1+z)^3}{1-\Omega_{m0}}\right) - {}_2F_1\left(\frac{1}{3}, \frac{1}{2}; \frac{4}{3}; -\frac{\Omega_{m0}}{1-\Omega_{m0}}\right) \right]^{-1}. \quad (2.9)$$

So, in the above equation, B is defined in such a way that its corresponding value for the Λ CDM model is 1 i.e.

$$B_{\Lambda\text{CDM}}^{\text{late-time}}(z) = 1. \quad (2.10)$$

Eq. (2.9) can be useful for the model-independent null test for the evidence of dynamical dark energy, especially, when BAO data is considered. Given the values of Ω_{m0} and $A(z)$ from any observations, we can compute $B(z)$ from Eq. (2.9) and if this value deviates from unity at late times, we get evidence for dynamical dark energy.

Later, we will see that $A(z)$ can be computed directly from the BAO observations, but the computation of Ω_{m0} is not very trivial, because it is a derived parameter. Hence late-time model independent computation of Ω_{m0} is non-trivial. However, it can be indirectly computed from the combined parameter $\Omega_{m0}h^2$ and h . Here, h is a parameter and it is related to H_0 as

$$H_0 = 100 h \text{ Km s}^{-1} \text{ Mpc}^{-1}. \quad (2.11)$$

We will see later that $\Omega_{m0}h^2$ can be computed from observations like CMB almost independent of any late-time cosmological model (it depends mainly on early universe physics). The parameter h can be obtained from any local measurement of H_0 , mentioned later. So, the computation of variable B , defined in Eq. (2.9), does not depend only on A and Ω_{m0} (it would be the case if we would do any model-dependent analysis), rather it depends on A , $\Omega_{m0}h^2$, and h , while we want to do a late-time model-independent analysis. So, for a late-time model-independent analysis, it is useful to rewrite the expression of B , defined in Eq. (2.9), in the following way

$$B(z) = \frac{z\sqrt{h^2 - \omega_{m0}} A(z)}{\sqrt{\omega_{m0}(1+z)^3 + h^2 - \omega_{m0}}} \times \left[(1+z) {}_2F_1\left(\frac{1}{3}, \frac{1}{2}; \frac{4}{3}; -\frac{\omega_{m0}(1+z)^3}{h^2 - \omega_{m0}}\right) - {}_2F_1\left(\frac{1}{3}, \frac{1}{2}; \frac{4}{3}; -\frac{\omega_{m0}}{h^2 - \omega_{m0}}\right) \right]^{-1}, \quad (2.12)$$

where ω_{m0} is given as

$$\omega_{m0} = \Omega_{m0}h^2. \quad (2.13)$$

So, from the values of A , ω_{m0} , and h from any combination of observations, we can compute B using Eq. (2.12) and check whether the computed value of B is consistent with 1 or it significantly deviates from 1. This will further tell us whether this particular combination of observations favors the Λ CDM model or not.

Besides the advantage that the diagnostic B (in Eq. (2.9) or in Eq. (2.12)) is independent of r_d , as already mentioned in the introduction, it can be more useful compared to other

Sr. No.	tracer (DESI24)	z_{eff}	$A \pm \Delta A$	Refs.
1	LRG	0.51	1.273 ± 0.052	[63]
2	LRG	0.71	1.182 ± 0.049	[63]
3	LRG+ELG	0.93	1.306 ± 0.036	[39]
4	ELG	1.32	1.523 ± 0.072	[64]
5	Ly- α	2.33	2.000 ± 0.075	[39]

Table 1. The measurements of $A = \frac{D_M}{zD_H}$ with 1σ error bars at five different effective redshifts corresponding to the DESI 2024 data (denoted as 'DESI24') [39].

diagnostics such as the Om diagnostic [59, 60], when we consider anisotropic BAO data because it takes into account anisotropic BAO data in both transverse and line of sight directions (i.e. $\frac{D_M}{r_d}$ and $\frac{D_H}{r_d}$ together) simultaneously at the same time. This advantage is not present in most of the diagnostics like Om diagnostic, where one can only consider one kind of anisotropic BAO data in a particular direction (i.e. either $\frac{D_M}{r_d}$ or $\frac{D_H}{r_d}$) at a time and mostly $\frac{D_H}{r_d}$ not $\frac{D_M}{r_d}$ because inclusion of $\frac{D_M}{r_d}$ may require its derivative which makes the analysis complicated. It would be even more complicated if one wants to include both $\frac{D_M}{r_d}$ and $\frac{D_H}{r_d}$ simultaneously at the same time.

3 Observational data

3.1 DESI 2024 BAO

We consider Dark Energy Spectroscopic Instrument (DESI) 2024 BAO observations [39] as the main data in our analysis. These data contain five main samples which are the Luminous Red Galaxy samples (LRG) at two effective redshifts $z_{\text{eff}} = 0.51$ and $z_{\text{eff}} = 0.71$ [63], combinations of LRG and the Emission Line Galaxy sample (ELG) at effective redshift $z_{\text{eff}} = 0.93$ [39], the solo ELG sample at effective redshift $z_{\text{eff}} = 1.32$ [64], and the Lyman- α forest sample (Ly- α) at effective redshift $z_{\text{eff}} = 2.33$ [39].

In Table 1, we list five different values of A i.e. $\frac{D_M}{zD_H}$ and the associated 1σ error bars at five different effective redshifts obtained from the DESI 2024 data [39]. We call these data 'DESI24' throughout this analysis. The Δ notation in front of any quantity corresponds to the standard deviation (1σ error) of that quantity throughout this paper. Note that, throughout the entire analysis, we use the notation '+' between any names of observations to convey that the observations have been combined for any analysis.

In Appendix B, we have included the methodology to compute the values of A and ΔA from the actual data of $\frac{D_M}{r_d}$ and $\frac{D_H}{r_d}$ of DESI 2024 BAO observations.

3.2 Planck CMB mission 2018: CMB distance priors

The cosmic microwave background (CMB) observations can be summarised through two main quantities: the CMB shift parameter R and the acoustic length scale l_A at photon decoupling redshift z_* [65–67]. The expressions of R and l_A are given as

$$R = \frac{\sqrt{\Omega_{\text{m}0} H_0^2} D_M(z_*)}{c}, \quad (3.1)$$

$$l_A = \frac{\pi D_M(z_*)}{r_s(z_*)}, \quad (3.2)$$

respectively, where r_s is the sound horizon. Dividing Eq. (3.1) by Eq. (3.2), we get the ratio Q given as

$$Q = \frac{R}{l_A} = \frac{\sqrt{\omega_{\text{m}0}} r_s(z_*)}{3000\pi \text{ Mpc}}, \quad (3.3)$$

where we have used the fact that

$$\frac{H_0}{c} \simeq \frac{h}{3000 \text{ Mpc}}. \quad (3.4)$$

The definition of Q in Eq. (3.3) is such that it is independent of late-time cosmological dynamics and it only depends on early-time physics. The mean values of Q and the corresponding 1σ error from Planck 2018 results for TT,TE,EE+lowE+lensing are given as [7]

$$Q = 0.005796 \pm 0.000016. \quad (3.5)$$

It can be shown that for standard early-time physics, $r_s(z_*)$ depends only on two parameters $\omega_{\text{m}0}$ and $\omega_{\text{b}0}$. Here, $\omega_{\text{b}0}$ is given as

$$\omega_{\text{b}0} = \Omega_{\text{b}0} h^2, \quad (3.6)$$

where $\Omega_{\text{b}0}$ is the baryon energy density parameter at present. For details, see Appendix C and Appendix D. Consequently, through Eq. (3.3), Q also depends only on these two parameters i.e.

$$Q \equiv Q(\omega_{\text{m}0}, \omega_{\text{b}0}). \quad (3.7)$$

The value of $\omega_{\text{b}0}$ is almost independent of late-time physics. For the standard early-time physics and the same CMB data, its value is given as [7]

$$\omega_{\text{b}0} = 0.02237 \pm 0.00015. \quad (3.8)$$

Considering values of Q and $\omega_{\text{b}0}$ from Eqs. (3.5) and (3.8) respectively and solving the equation in Eq. (3.7), we get a mean value of $\omega_{\text{m}0}$ and the corresponding 1σ error given as

$$\omega_{\text{m}0} = 0.1429 \pm 0.0014. \quad (3.9)$$

We call this CMB data the 'Pl18(standard)' throughout this analysis.

We also consider a non-standard early universe cosmology by allowing variations in the sum of neutrino masses Σm_ν and effective number of relativistic species N_{eff} . With a similar procedure and following Zhai et al. (2020), we have [66]

$$\omega_{\text{m}0} = 0.1413 \pm 0.0039. \quad (3.10)$$

We call this CMB data as 'Pl18(standard+ $\Sigma m_\nu + N_{\text{eff}}$)' throughout the analysis.

We list two values of $\omega_{\text{m}0}$, obtained from Eqs. (3.9) and (3.10), in Table 2.

Sr. No.	Observation	$\omega_{m0} \pm \Delta\omega_{m0}$
1	Pl18(standard)	0.1429 ± 0.0014
2	Pl18(standard+ $\Sigma m_\nu + N_{\text{eff}}$)	0.1413 ± 0.0039

Table 2. The two values of ω_{m0} , obtained from Eq. (3.9) (using Planck 2018 results for TT,TE,EE+lowE+lensing with standard early time physics, denoted by 'Pl18(standard)') and Eq. (3.10) (using Planck 2018 results for TT,TE,EE+lowE+lensing with a non-standard early universe cosmology by allowing variations in sum of neutrino masses Σm_ν and effective number of relativistic species N_{eff} , denoted by 'Pl18(standard+ $\Sigma m_\nu + N_{\text{eff}}$)').

Sr. No.	Observation	$h \pm \Delta h$	Refs.
1	H_0 (tRGB)	0.698 ± 0.019	[68]
2	H_0 (SHOES)	0.732 ± 0.013	[31]

Table 3. The two values of h , obtained from tRGB and SHOES data, are denoted by ' H_0 (tRGB)' and ' H_0 (SHOES)' respectively.

3.3 H_0 measurements

To compute the diagnostic parameter B in Eq. (2.12), we need the values of the h parameter. Hence, we need the values of the H_0 parameter. Note that, even if we consider the alternative expression of B in Eq. (2.9), we still require a value of h . This is because CMB observations provide the combination $\Omega_{m0}h^2$, not directly Ω_{m0} . So, to break the degeneracy of $\Omega_{m0}h^2$ to get Ω_{m0} , we require the value of h . Anyway, theoretically, the diagnostic parameter B can be independent of h through Eq. (2.9), only if any observations directly provide a value of the Ω_{m0} parameter independent of h . To the best of our knowledge, we believe, there are no such observations which do so. Thus, the expression of diagnostic variable B in Eq. (2.12) is practically more useful than the one in Eq. (2.9) and this variable depends on the value of h . For this purpose, we consider two observations: the tip of the Red Giant Branch (tRGB) which corresponds to $H_0 = 69.8 \pm 1.9$ [Km s⁻¹ Mpc⁻¹] i.e. $h = 0.698 \pm 0.019$ [68] and the SHOES observations which correspond to $H_0 = 73.2 \pm 1.3$ [Km s⁻¹ Mpc⁻¹] i.e. $h = 0.732 \pm 0.013$ [31]. We call these data as ' H_0 (tRGB)' and ' H_0 (SHOES)' respectively.

We list these two values of h in Table 3.

3.4 Other BAO data

Besides, DESI 2024 data, we also consider other (non-DESI) BAO observations [69]. For this data, we closely follow Alam et al. (2020) [9] which corresponds to the completed Sloan Digital Sky Survey (SDSS) IV. We consider five pairs of measurements of $\frac{D_M}{r_d}$ and $\frac{D_H}{r_d}$ at five effective redshifts. The first and second pairs correspond to the Baryon Oscillation Spectroscopic Survey (BOSS) DR12 LRG sample at effective redshifts 0.38 and 0.51 respectively [8]. The third pair corresponds to the extended Baryon Oscillation Spectroscopic Survey (eBOSS) DR16 LRG sample at effective redshift 0.698 [9]. The fourth pair corresponds to the eBOSS DR16 QSO sample at effective redshift 1.48 [70]. The fifth pair corresponds to eBOSS DR16 Ly- α QSO sample at effective redshift 2.334 [71]. From $\frac{D_M}{r_d}$ and $\frac{D_H}{r_d}$ pair, we compute A and ΔA at each effective redshift using second equality of Eq. (2.7) and the corresponding propagation of uncertainty. In Appendix B, we have included the methodology to compute the values of A and ΔA from the actual data of $\frac{D_M}{r_d}$ and $\frac{D_H}{r_d}$ of these BAO observations. All

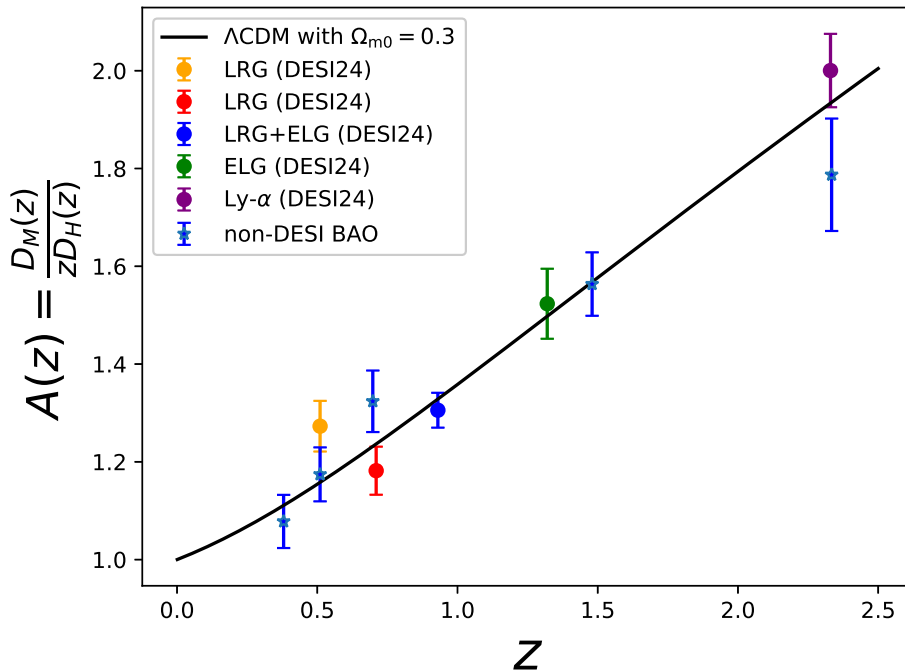


Figure 1. Error bars plot corresponding to A and ΔA both for DESI 2024 (denoted by 'DESI24') and other BAO (denoted by 'non-DESI BAO') data. The continuous black line is a reference plot for $A(z)$ vs. z for the Λ CDM model with $\Omega_{m0} = 0.3$ using Eq. (2.8). All the blue-colored error bars with the asterisk sign for the mean values of A correspond to the other BAO data (non-DESI BAO), obtained from Table 4. All other error bars with different colors correspond to the DESI 2024 BAO data (DESI24), obtained from Table 1. The orange, red, blue, green, and purple colored error bars correspond to the DESI24 data at effective redshifts 0.51 (LRG), 0.71 (LRG), 0.93 (LRG+ELG), 1.32 (ELG), and 2.33 (Ly- α) respectively.

Sr. No.	tracer (non-DESI BAO)	z_{eff}	$A \pm \Delta A$	Refs.
1	LRG (BOSS DR12)	0.38	1.078 ± 0.054	[8]
2	LRG (BOSS DR12)	0.51	1.174 ± 0.055	[8]
3	LRG (eBOSS DR16)	0.698	1.324 ± 0.063	[9]
4	QSO (eBOSS DR16)	1.48	1.564 ± 0.065	[70]
5	Ly- α QSO (eBOSS DR16)	2.334	1.787 ± 0.115	[71]

Table 4. The measurements of $A = \frac{D_M}{z D_H}$ with 1σ error bars at five different effective redshifts corresponding to other BAO data (denoted as 'non-DESI BAO') [9].

these values are listed in Table 4. Note that, while we compute ΔA using propagation of uncertainty, we have included the covariances between $\frac{D_M}{r_d}$ and $\frac{D_H}{r_d}$. We denote these BAO data as 'non-DESI BAO'.

To check the values of the quantity A , obtained from different BAO observations, compared to the standard Λ CDM model, we plot all these values in Fig. 1 with error bars. The continuous black line is for the Λ CDM model with $\Omega_{m0} = 0.3$ obtained using Eq. (2.8). We plot all the non-DESI BAO data with the same color with the blue colored error bars with

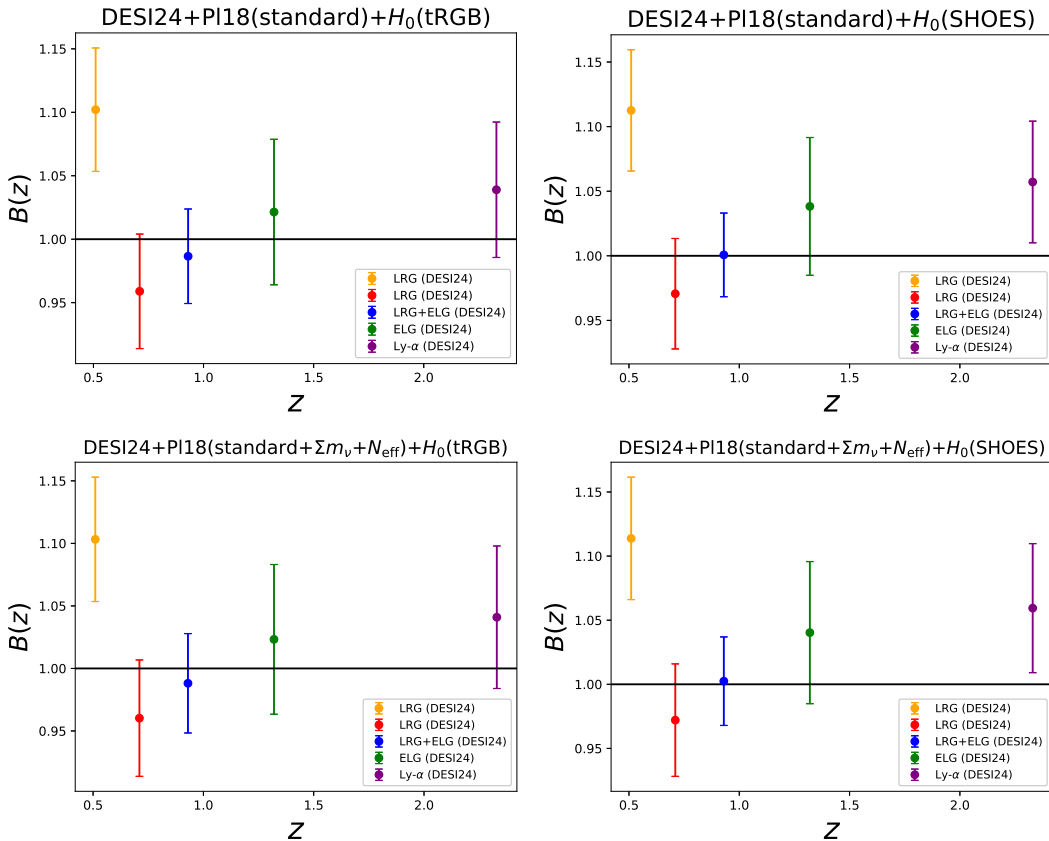


Figure 2. Plots of the diagnostic variable $B(z)$ and the associated 1σ errors. These values are obtained from DESI 2024 (DESI24) data combined with CMB and H_0 measurements using Eq. (2.12) (with A values obtained from Table 1, ω_{m0} values obtained from Table 2, and h values obtained from Table 3).

the asterisk sign for the mean values of A , obtained from Table 4. For the DESI24 data, we use different colors for different values of A and ΔA at different effective redshifts, obtained from Table 1. The orange, red, blue, green, and purple colored error bars correspond to the DESI24 data at effective redshifts 0.51 (LRG), 0.71 (LRG), 0.93 (LRG+ELG), 1.32 (ELG), and 2.33 (Ly- α) respectively. We use the same color combinations in all other figures when we refer to the BAO data (both DESI24 and non-DESI BAO).

4 Results

Combining ω_{m0} , obtained from CMB observations, listed in Table 2 and h from H_0 observations, listed in Table 3, we can compute the mean values of Ω_{m0} parameter and the corresponding 1σ errors. We list these values in Table 5.

By using the values of $A(z)$ from Table 1 and Ω_{m0} from Table 5, we can compute $B(z)$ at each redshift with each value of Ω_{m0} using Eq. (2.9) and the corresponding error ΔB using propagation of uncertainty. Alternatively, by using the values of $A(z)$ from Table 1, the values of ω_{m0} from Table 2 and the values of h from Table 3, we compute $B(z)$ at each redshift using Eq. (2.12) and the corresponding error ΔB using propagation of uncertainty. These two procedures give completely equivalent results, but the only difference is that we

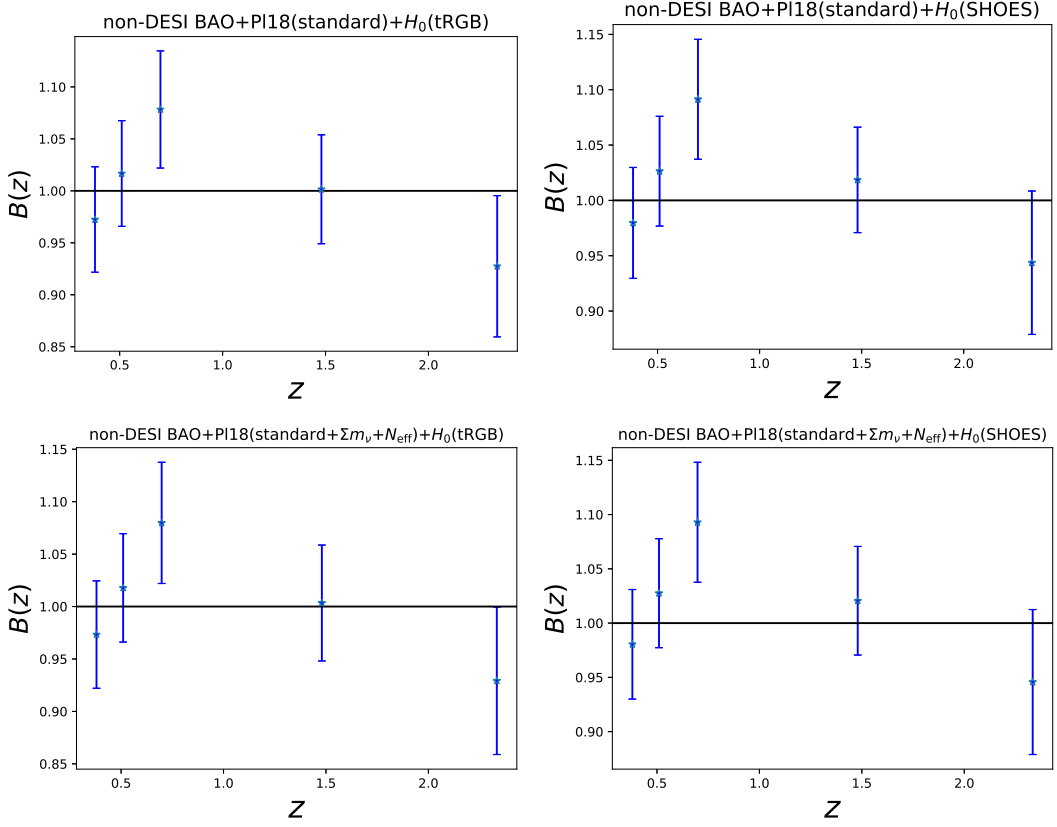


Figure 3. Plots of the diagnostic variable $B(z)$ and the associated 1σ errors. These values are obtained from non-DESI BAO data combined with CMB and H_0 measurements using Eq. (2.12) (with A values obtained from Table 4, ω_{m0} values obtained from Table 2, and h values obtained from Table 3).

Sr. No.	Data combinations	$\Omega_{m0} \pm \Delta\Omega_{m0}$
1	Pl18(standard)+ H_0 (tRGB)	0.293 ± 0.016
2	Pl18(standard)+ H_0 (SHOES)	0.267 ± 0.010
3	Pl18(standard+ $\Sigma m_\nu + N_{\text{eff}}$)+ H_0 (tRGB)	0.290 ± 0.018
4	Pl18(standard+ $\Sigma m_\nu + N_{\text{eff}}$)+ H_0 (SHOES)	0.264 ± 0.012

Table 5. Four different values of Ω_{m0} parameter and the corresponding 1σ errors were obtained from four different combinations of data sets.

can visualize the h dependence directly when we follow the second procedure i.e. when we use Eq. (2.12).

We plot the computed values of B and ΔB in Fig. 2 with the help of error bar plots. The significance of these plots is such that any deviation from $B = 1$ corresponds to the deviation from the standard Λ CDM model. So, these plots correspond to the model-independent null test of evidence for the dynamical dark energy.

First of all, in Fig. 2, when we compare the top-left panel with the bottom-left panel and the top-right panel with the bottom-right panel, we can see that the results are almost

Sr. No.	Data combinations	$\langle\sigma_d\rangle$	$\langle\sigma_d\rangle$ (without 0.51)
1	DESI24+P118(standard)+ H_0 (tRGB)	0.9	0.6
2	DESI24+P118(standard)+ H_0 (SHOES)	1.0	0.7
3	DESI24+P118(standard+ $\Sigma m_\nu+N_{\text{eff}}$)+ H_0 (tRGB)	0.9	0.6
4	DESI24+P118(standard+ $\Sigma m_\nu+N_{\text{eff}}$)+ H_0 (SHOES)	1.0	0.7

Table 6. Average σ deviation $\langle\sigma_d\rangle$ (obtained using Eq. (4.1)) of the Λ CDM model from the observed best-fit values of B for four different combinations of data sets corresponding to each panel of Fig. 2 (involving DESI 2024 (DESI24) data combined with CMB and H_0 measurements). We have also quoted the corresponding values excluding the redshift point 0.51.

similar. This means the deviations of $B(z)$ from the value 1 i.e. the deviations from the Λ CDM model are almost independent of the early-time physics (irrespective of whether we consider standard early-time physics or the early cosmological model with the varying sum of neutrino masses Σm_ν and effective number of relativistic species N_{eff}).

Now, if we compare the left panels with the right panels in Fig. 2, we can see that the deviations are slightly different. This means these deviations slightly depend on the values of H_0 . This is simply because the estimation of $\Omega_{\text{m}0}$ depends on H_0 . However, these differences are very small.

Next, from Fig. 2, we can see that the horizontal black lines ($B = 1$) are almost 2σ away from the estimated values of B at $z = 0.51$ (the first points with the orange colored error bars corresponding to the LRG sample of DESI24 observations). The horizontal black lines are around 1σ (precisely little less than 1σ) away from the estimated values of B at $z = 0.71$ (the second points with the red colored error bars corresponding to the LRG sample of DESI24 observations) and $z = 2.33$ (the fifth points with the purple colored error bars corresponding to the Ly- α QSO sample of DESI24 observations). At the other two redshift points, the deviations are well within 1σ error bars. This means there is slight evidence for the dynamical dark energy.

However, the quantification of each deviation at each redshift is not that useful to make any conclusion unless we quantify an average deviation, obtained from the combination of all the deviations at all redshifts. To do so, we quantify the average σ deviation using a quantity $\langle\sigma_d\rangle$ given as

$$\langle\sigma_d\rangle = \frac{1}{N} \sum_{i=1}^N \frac{|B(z_i) - 1|}{\Delta B(z_i)}, \quad (4.1)$$

where N is the number of all the redshift points where each deviations are computed. Clearly, in this analysis, $N = 5$. Here, z_i denotes each redshift point corresponding to either Fig. 2 or Fig. 3. We list all the obtained values of average sigma deviation $\langle\sigma_d\rangle$ corresponding to each panel of Fig. 2 in Table 6.

From Table 6, we can see that the average deviations of $B = 1$ (the Λ CDM value) from the best-fit values of B obtained from the different combinations of data involving DESI24, CMB, and H_0 measurements are almost 1σ away. These deviations are a little lesser when we exclude the LRG sample of DESI24 data at effective redshift 0.51, but not significantly different (only around 0.3σ less). Similar to the individual deviations at each redshift, the average deviations are almost independent of the early-time dynamics and have little dependence on the values of H_0 (differences are only around 0.1σ).

Sr. No.	Data combinations	$\langle\sigma_d\rangle$
1	non-DESI BAO+P118(standard)+ H_0 (tRGB)	0.7
2	non-DESI BAO+P118(standard)+ H_0 (SHOES)	0.8
3	non-DESI BAO+P118(standard+ $\Sigma m_\nu+N_{\text{eff}}$)+ H_0 (tRGB)	0.7
4	non-DESI BAO+P118(standard+ $\Sigma m_\nu+N_{\text{eff}}$)+ H_0 (SHOES)	0.8

Table 7. Average σ deviation $\langle\sigma_d\rangle$ (obtained using Eq. (4.1)) of the Λ CDM model from the observed best-fit values of B for four different combinations of data sets corresponding to each panel of Fig. 3 (involving non-DESI BAO data combined with CMB and H_0 measurements).

In summary, we get low to moderate evidence of dynamical dark energy when we combine the DESI24 data, the CMB observations from the Planck 2018 mission, and the H_0 values from the local measurements. This evidence is not that strong compared to the evidence (more than 2σ) obtained from the DESI key paper Adame et al. (2024) (DESI Collaboration) [39] with the w_0w_a CDM parametrization of dark energy equation of state parameter. While the results from this model-independent null test are not consistent with the results obtained from the DESI key paper for the w_0w_a CDM parametrization, interestingly, our results are more or less consistent with the results of the DESI key paper for the $w_p \equiv w(z_p)$ parametrization (or the z_pw_p CDM parametrization, an alternative parametrization to the w_0w_a CDM parametrization with z_p being the pivot redshift), in which the Λ CDM model is around 1σ away except for the combination 'DESI+CMB+DESY5' in the DESI key paper (see equation (5.9) in DESI key paper Adame et al. (2024) (DESI Collaboration) [39]). For a quick overview, in Appendix E, we have included a brief discussion about w CDM, w_0w_a CDM [34, 35], and z_pw_p CDM [72, 73] parametrizations.

Now, we turn our attention to the other non-DESI BAO data combined with the same CMB and H_0 data. We draw similar plots of diagnostic variable $B(z)$ and the associated 1σ errors in Fig. 3, obtained from non-DESI BAO data combined with CMB and H_0 measurements using Eq. (2.12) (with A values obtained from Table 4, ω_{m0} values obtained from Table 2, and h values obtained from Table 3). Here, also, we see individual deviations in Fig. 3 are almost independent of the early-time physics, while there is little dependence on the H_0 values, but not so significant. We also compute the average σ deviation $\langle\sigma_d\rangle$ (obtained using Eq. (4.1)) of the Λ CDM model from the observed best-fit values of B corresponding to each panel of Fig. 3. We list these values in Table 7.

From Table 7, we see that the average deviations are almost similar in all combinations of data. So, the evidence of dynamical dark energy is almost independent of the early-time physics and the H_0 values. Interestingly, we see that the deviations are almost similar compared to the DESI24 data excluding redshift point 0.51 of DESI24 data. Even if we compare the results with the inclusion of redshift point 0.51 of DESI24 data, the average deviations are not significantly different (only around 0.2σ difference).

So, with the analysis, presented in this study, with the diagnostic null test, we find low to moderate evidence of dynamical dark energy both for DESI 2024 and other BAO data but not very significant.

5 Conclusion

We have proposed a new diagnostic for the null test for the evidence of dynamical dark energy. This diagnostic measures the deviation from the Λ CDM model for the late-time background evolution of the Universe. This diagnostic is independent of any late-time cosmological model or parametrization, however, the derivation of this diagnostic depends on the basic cosmological assumptions that the background geometry of the Universe is described by the flat FLRW metric. This kind of null test is crucial to avoid any model-dependent bias, any dependence on priors of the dark energy model parameters, and the presence of any degeneracies in the estimations of the dark energy parameters.

We have defined the diagnostic by a quantity B as a function of redshift. For the Λ CDM model of the late-time background dynamics of the Universe, the value of this quantity is unity i.e. $B = 1$ at any redshift. The deviation in the observed value of B , obtained from any observations, from $B = 1$ corresponds to the deviation from the Λ CDM model. Thus, any significant deviations from $B = 1$ correspond to the evidence for the dynamical dark energy.

With this diagnostic, we study the deviations from the Λ CDM model with the combinations of the latest anisotropic BAO measurements from DESI 2024 DR1 data, CMB data from Planck 2018 mission (TT,TE,EE+lowE+lensing), and local measurements of H_0 (both from tRGB and SHOES observations). We also consider other BAO observations mostly from SDSS IV data in our analysis.

When DESI 2024 and the CMB observations are combined with the H_0 measurement of tRGB observations, the Λ CDM model is less than 1σ away from most of the best-fit values of B (except the one at $z = 0.51$ where it is around 2σ away corresponding to the LRG sample of DESI 2024 data). We also compute the average deviations combining all the deviations from each redshift. We find the Λ CDM model is around 0.9σ away when we combine all five DESI 2024 data and it is 0.6σ away when we exclude the LRG sample at effective redshift 0.51. When we replace the tRGB H_0 value with SHOES H_0 value, we get slight differences in the individual deviations, but the average deviations are almost similar. In this case, the Λ CDM model is around 1σ (including redshift 0.51) and 0.7σ (excluding redshift 0.51) away respectively. This means the evidence for dynamical dark energy is low to moderate but not very significant.

When we consider other BAO data instead of DESI 2024 data, we see exactly similar results compared to the DESI 2024 data (excluding redshift 0.51). Even if we compare with the DESI BAO data including redshift 0.51, the differences are only 0.2σ .

We find all the deviations (both at individual redshift points and the average ones) are almost independent of any early-time physics.

While the results, in this analysis, are not consistent with w_0w_a CDM model results of the DESI key paper, but interestingly, all these results are very consistent with the results with z_pw_p CDM model of the DESI key paper.

Acknowledgments

The author is supported by the South African Radio Astronomy Observatory and National Research Foundation (Grant No. 75415). The author would like to thank Roy Maartens for useful comments on the draft.

References

- [1] **Supernova Cosmology Project** Collaboration, S. Perlmutter et al., *Discovery of a supernova explosion at half the age of the Universe and its cosmological implications*, *Nature* **391** (1998) 51–54, [[astro-ph/9712212](#)].
- [2] **Supernova Search Team** Collaboration, A. G. Riess et al., *Observational evidence from supernovae for an accelerating universe and a cosmological constant*, *Astron. J.* **116** (1998) 1009–1038, [[astro-ph/9805201](#)].
- [3] **Supernova Cosmology Project** Collaboration, S. Perlmutter et al., *Measurements of Ω and Λ from 42 high redshift supernovae*, *Astrophys. J.* **517** (1999) 565–586, [[astro-ph/9812133](#)].
- [4] A. Wright, *Nobel Prize 2011: Perlmutter, Schmidt & Riess*, *Nature Physics* **7** (Nov., 2011) 833.
- [5] **Planck** Collaboration, P. A. R. Ade et al., *Planck 2013 results. XVI. Cosmological parameters*, *Astron. Astrophys.* **571** (2014) A16, [[arXiv:1303.5076](#)].
- [6] **Planck** Collaboration, P. A. R. Ade et al., *Planck 2015 results. XIII. Cosmological parameters*, *Astron. Astrophys.* **594** (2016) A13, [[arXiv:1502.01589](#)].
- [7] **Planck** Collaboration, N. Aghanim et al., *Planck 2018 results. VI. Cosmological parameters*, *Astron. Astrophys.* **641** (2020) A6, [[arXiv:1807.06209](#)]. [Erratum: *Astron. Astrophys.* 652, C4 (2021)].
- [8] **BOSS** Collaboration, S. Alam et al., *The clustering of galaxies in the completed SDSS-III Baryon Oscillation Spectroscopic Survey: cosmological analysis of the DR12 galaxy sample*, *Mon. Not. Roy. Astron. Soc.* **470** (2017), no. 3 2617–2652, [[arXiv:1607.03155](#)].
- [9] **eBOSS** Collaboration, S. Alam et al., *Completed SDSS-IV extended Baryon Oscillation Spectroscopic Survey: Cosmological implications from two decades of spectroscopic surveys at the Apache Point Observatory*, *Phys. Rev. D* **103** (2021), no. 8 083533, [[arXiv:2007.08991](#)].
- [10] J. Hou et al., *The Completed SDSS-IV extended Baryon Oscillation Spectroscopic Survey: BAO and RSD measurements from anisotropic clustering analysis of the Quasar Sample in configuration space between redshift 0.8 and 2.2*, *Mon. Not. Roy. Astron. Soc.* **500** (2020), no. 1 1201–1221, [[arXiv:2007.08998](#)].
- [11] R. Jimenez and A. Loeb, *Constraining cosmological parameters based on relative galaxy ages*, *Astrophys. J.* **573** (2002) 37–42, [[astro-ph/0106145](#)].
- [12] A. M. Pinho, S. Casas, and L. Amendola, *Model-independent reconstruction of the linear anisotropic stress η* , *JCAP* **11** (2018) 027, [[arXiv:1805.00027](#)].
- [13] S. Cao and B. Ratra, *$H_0=69.8\pm 1.3$ km s⁻¹ Mpc⁻¹, $\Omega_{m0}=0.288\pm 0.017$, and other constraints from lower-redshift, non-CMB, expansion-rate data*, *Phys. Rev. D* **107** (2023), no. 10 103521, [[arXiv:2302.14203](#)].
- [14] P. J. E. Peebles and B. Ratra, *The Cosmological Constant and Dark Energy*, *Rev. Mod. Phys.* **75** (2003) 559–606, [[astro-ph/0207347](#)].
- [15] E. J. Copeland, M. Sami, and S. Tsujikawa, *Dynamics of dark energy*, *Int. J. Mod. Phys. D* **15** (2006) 1753–1936, [[hep-th/0603057](#)].
- [16] J. Yoo and Y. Watanabe, *Theoretical Models of Dark Energy*, *Int. J. Mod. Phys. D* **21** (2012) 1230002, [[arXiv:1212.4726](#)].
- [17] A. I. Lonappan, S. Kumar, Ruchika, B. R. Dinda, and A. A. Sen, *Bayesian evidences for dark energy models in light of current observational data*, *Phys. Rev. D* **97** (2018), no. 4 043524, [[arXiv:1707.00603](#)].
- [18] B. R. Dinda, *Probing dark energy using convergence power spectrum and bi-spectrum*, *JCAP* **09** (2017) 035, [[arXiv:1705.00657](#)].

- [19] B. R. Dinda, A. A. Sen, and T. R. Choudhury, *Dark energy constraints from the 21 cm intensity mapping surveys with SKA1*, [arXiv:1804.11137](#).
- [20] K. Bamba, S. Capozziello, S. Nojiri, and S. D. Odintsov, *Dark energy cosmology: the equivalent description via different theoretical models and cosmography tests*, *Astrophys. Space Sci.* **342** (2012) 155–228, [[arXiv:1205.3421](#)].
- [21] B. R. Dinda and N. Banerjee, *A comprehensive data-driven odyssey to explore the equation of state of dark energy*, [arXiv:2403.14223](#).
- [22] S. M. Carroll, *The Cosmological constant*, *Living Rev. Rel.* **4** (2001) 1, [[astro-ph/0004075](#)].
- [23] I. Zlatev, L.-M. Wang, and P. J. Steinhardt, *Quintessence, cosmic coincidence, and the cosmological constant*, *Phys. Rev. Lett.* **82** (1999) 896–899, [[astro-ph/9807002](#)].
- [24] V. Sahni and A. A. Starobinsky, *The Case for a positive cosmological Lambda term*, *Int. J. Mod. Phys. D* **9** (2000) 373–444, [[astro-ph/9904398](#)].
- [25] H. Velten, R. vom Marttens, and W. Zimdahl, *Aspects of the cosmological “coincidence problem”*, *Eur. Phys. J. C* **74** (2014), no. 11 3160, [[arXiv:1410.2509](#)].
- [26] M. Malquarti, E. J. Copeland, and A. R. Liddle, *K-essence and the coincidence problem*, *Phys. Rev. D* **68** (2003) 023512, [[astro-ph/0304277](#)].
- [27] E. Di Valentino, O. Mena, S. Pan, L. Visinelli, W. Yang, A. Melchiorri, D. F. Mota, A. G. Riess, and J. Silk, *In the realm of the Hubble tension—a review of solutions*, *Class. Quant. Grav.* **38** (2021), no. 15 153001, [[arXiv:2103.01183](#)].
- [28] C. Krishnan, R. Mohayaee, E. O. Colgáin, M. M. Sheikh-Jabbari, and L. Yin, *Does Hubble tension signal a breakdown in FLRW cosmology?*, *Class. Quant. Grav.* **38** (2021), no. 18 184001, [[arXiv:2105.09790](#)].
- [29] S. Vagnozzi, *New physics in light of the H_0 tension: An alternative view*, *Phys. Rev. D* **102** (2020), no. 2 023518, [[arXiv:1907.07569](#)].
- [30] B. R. Dinda, *Cosmic expansion parametrization: Implication for curvature and H_0 tension*, *Phys. Rev. D* **105** (2022), no. 6 063524, [[arXiv:2106.02963](#)].
- [31] A. G. Riess, S. Casertano, W. Yuan, J. B. Bowers, L. Macri, J. C. Zinn, and D. Scolnic, *Cosmic Distances Calibrated to 1% Precision with Gaia EDR3 Parallaxes and Hubble Space Telescope Photometry of 75 Milky Way Cepheids Confirm Tension with Λ CDM*, *Astrophys. J. Lett.* **908** (2021), no. 1 L6, [[arXiv:2012.08534](#)].
- [32] B. R. Dinda and A. A. Sen, *Imprint of thawing scalar fields on the large scale galaxy overdensity*, *Phys. Rev. D* **97** (2018), no. 8 083506, [[arXiv:1607.05123](#)].
- [33] B. R. Dinda and N. Banerjee, *Constraints on the speed of sound in the k-essence model of dark energy*, *Eur. Phys. J. C* **84** (2024), no. 2 177, [[arXiv:2309.10538](#)].
- [34] M. Chevallier and D. Polarski, *Accelerating universes with scaling dark matter*, *Int. J. Mod. Phys. D* **10** (2001) 213–224, [[gr-qc/0009008](#)].
- [35] E. V. Linder, *Exploring the expansion history of the universe*, *Phys. Rev. Lett.* **90** (2003) 091301, [[astro-ph/0208512](#)].
- [36] D. Brout et al., *The Pantheon+ Analysis: Cosmological Constraints*, *Astrophys. J.* **938** (2022), no. 2 110, [[arXiv:2202.04077](#)].
- [37] D. Rubin et al., *Union Through UNITY: Cosmology with 2,000 SNe Using a Unified Bayesian Framework*, [arXiv:2311.12098](#).
- [38] **DES** Collaboration, T. M. C. Abbott et al., *The Dark Energy Survey: Cosmology Results With ~ 1500 New High-redshift Type Ia Supernovae Using The Full 5-year Dataset*, [arXiv:2401.02929](#).

- [39] DESI Collaboration, A. G. Adame et al., *DESI 2024 VI: Cosmological Constraints from the Measurements of Baryon Acoustic Oscillations*, [arXiv:2404.03002](#).
- [40] D. Wang, *The Self-Consistency of DESI Analysis and Comment on "Does DESI 2024 Confirm Λ CDM?"*, [arXiv:2404.13833](#).
- [41] C.-G. Park, J. de Cruz Perez, and B. Ratra, *Using non-DESI data to confirm and strengthen the DESI 2024 spatially-flat w_0w_a CDM cosmological parameterization result*, [arXiv:2405.00502](#).
- [42] Y. Tada and T. Terada, *Quintessential interpretation of the evolving dark energy in light of DESI*, [arXiv:2404.05722](#).
- [43] D. Wang, *Constraining Cosmological Physics with DESI BAO Observations*, [arXiv:2404.06796](#).
- [44] Y. Carloni, O. Luongo, and M. Muccino, *Does dark energy really revive using DESI 2024 data?*, [arXiv:2404.12068](#).
- [45] K. V. Berghaus, J. A. Kable, and V. Miranda, *Quantifying Scalar Field Dynamics with DESI 2024 Y1 BAO measurements*, [arXiv:2404.14341](#).
- [46] W. Giarè, M. A. Sabogal, R. C. Nunes, and E. Di Valentino, *Interacting Dark Energy after DESI Baryon Acoustic Oscillation measurements*, [arXiv:2404.15232](#).
- [47] F. J. Qu, K. M. Surrao, B. Bolliet, J. C. Hill, B. D. Sherwin, and H. T. Jense, *Accelerated inference on accelerated cosmic expansion: New constraints on axion-like early dark energy with DESI BAO and ACT DR6 CMB lensing*, [arXiv:2404.16805](#).
- [48] H. Wang and Y.-S. Piao, *Dark energy in light of recent DESI BAO and Hubble tension*, [arXiv:2404.18579](#).
- [49] Y. Yang, X. Ren, Q. Wang, Z. Lu, D. Zhang, Y.-F. Cai, and E. N. Saridakis, *Quintom cosmology and modified gravity after DESI 2024*, [arXiv:2404.19437](#).
- [50] W. Yin, *Cosmic Clues: DESI, Dark Energy, and the Cosmological Constant Problem*, [arXiv:2404.06444](#).
- [51] C. Escamilla-Rivera and R. Sandoval-Orozco, *$f(T)$ gravity after DESI Baryon Acoustic Oscillation and DES Supernovae 2024 data*, [arXiv:2405.00608](#).
- [52] Z. Huang et al., *MEET-U Project I: The key drivers of the preference for dynamic dark energy*, [arXiv:2405.03983](#).
- [53] E. O. Colgáin, M. G. Dainotti, S. Capozziello, S. Pourojaghi, M. M. Sheikh-Jabbari, and D. Stojkovic, *Does DESI 2024 Confirm Λ CDM?*, [arXiv:2404.08633](#).
- [54] R. Calderon et al., *DESI 2024: Reconstructing Dark Energy using Crossing Statistics with DESI DR1 BAO data*, [arXiv:2405.04216](#).
- [55] O. Luongo and M. Muccino, *Model independent cosmographic constraints from DESI 2024*, [arXiv:2404.07070](#).
- [56] E. V. Linder, *Biased Cosmology: Pivots, Parameters, and Figures of Merit*, *Astropart. Phys.* **26** (2006) 102–110, [[astro-ph/0604280](#)].
- [57] M. Cortês and A. R. Liddle, *Interpreting DESI's evidence for evolving dark energy*, [arXiv:2404.08056](#).
- [58] D. Shlivko and P. Steinhardt, *Assessing observational constraints on dark energy*, [arXiv:2405.03933](#).
- [59] V. Sahni, A. Shafieloo, and A. A. Starobinsky, *Two new diagnostics of dark energy*, *Phys. Rev. D* **78** (2008) 103502, [[arXiv:0807.3548](#)].

- [60] N. Myrzakulov, M. Koussour, and D. J. Gogoi, *A new $Om(z)$ diagnostic of dark energy in general relativity theory*, *Eur. Phys. J. C* **83** (2023), no. 7 594, [[arXiv:2303.04640](#)].
- [61] D. W. Hogg, *Distance measures in cosmology*, [astro-ph/9905116](#).
- [62] E. O. Colgáin, M. M. Sheikh-Jabbari, R. Solomon, G. Bargiacchi, S. Capozziello, M. G. Dainotti, and D. Stojkovic, *Revealing intrinsic flat Λ CDM biases with standardizable candles*, *Phys. Rev. D* **106** (2022), no. 4 L041301, [[arXiv:2203.10558](#)].
- [63] **DESI** Collaboration, R. Zhou et al., *Target Selection and Validation of DESI Luminous Red Galaxies*, *Astron. J.* **165** (2023), no. 2 58, [[arXiv:2208.08515](#)].
- [64] A. Raichoor et al., *Target Selection and Validation of DESI Emission Line Galaxies*, *Astron. J.* **165** (2023), no. 3 126, [[arXiv:2208.08513](#)].
- [65] L. Chen, Q.-G. Huang, and K. Wang, *Distance Priors from Planck Final Release*, *JCAP* **02** (2019) 028, [[arXiv:1808.05724](#)].
- [66] Z. Zhai, C.-G. Park, Y. Wang, and B. Ratra, *CMB distance priors revisited: effects of dark energy dynamics, spatial curvature, primordial power spectrum, and neutrino parameters*, *JCAP* **07** (2020) 009, [[arXiv:1912.04921](#)].
- [67] Z. Zhai and Y. Wang, *Robust and model-independent cosmological constraints from distance measurements*, *JCAP* **07** (2019) 005, [[arXiv:1811.07425](#)].
- [68] W. L. Freedman et al., *The Carnegie-Chicago Hubble Program. VIII. An Independent Determination of the Hubble Constant Based on the Tip of the Red Giant Branch*, *Astrophys. J.* **882** (2019) 34, [[arXiv:1907.05922](#)].
- [69] J. de Cruz Perez, C.-G. Park, and B. Ratra, *Updated observational constraints on spatially-flat and non-flat Λ CDM and X CDM cosmological models*, [arXiv:2404.19194](#).
- [70] **eBOSS** Collaboration, J. Hou et al., *The Completed SDSS-IV extended Baryon Oscillation Spectroscopic Survey: BAO and RSD measurements from anisotropic clustering analysis of the Quasar Sample in configuration space between redshift 0.8 and 2.2*, *Mon. Not. Roy. Astron. Soc.* **500** (2020), no. 1 1201–1221, [[arXiv:2007.08998](#)].
- [71] **eBOSS** Collaboration, H. du Mas des Bourboux et al., *The Completed SDSS-IV Extended Baryon Oscillation Spectroscopic Survey: Baryon Acoustic Oscillations with Ly α Forests*, *Astrophys. J.* **901** (2020), no. 2 153, [[arXiv:2007.08995](#)].
- [72] A. Albrecht et al., *Report of the Dark Energy Task Force*, [astro-ph/0609591](#).
- [73] D. Huterer and M. S. Turner, *Probing the dark energy: Methods and strategies*, *Phys. Rev. D* **64** (2001) 123527, [[astro-ph/0012510](#)].

A Analytical expression of comoving distance in Λ CDM model

In a flat FLRW cosmological background, the transverse comoving distance is equal to the line of sight comoving distance and in the Λ CDM model it is given as (by putting Eq. (2.2) in Eq. (2.1))

$$D_{M \Lambda\text{CDM}}^{\text{late-time}}(z) = \frac{c}{H_0} I(z), \quad (\text{A.1})$$

where I is given as

$$I(z) = \int_0^z \frac{d\tilde{z}}{\sqrt{\Omega_{m0}(1+\tilde{z})^3 + 1 - \Omega_{m0}}} . \quad (\text{A.2})$$

Now let us define α and β as

$$\alpha = \frac{1}{\sqrt{1 - \Omega_{\text{m}0}}}, \quad (\text{A.3})$$

$$\beta = -\frac{\Omega_{\text{m}0}}{1 - \Omega_{\text{m}0}}, \quad (\text{A.4})$$

respectively. With α and β , $I(z)$ in Eq. (A.2) can be rewritten as

$$I(z) = \alpha \int_0^z [1 - \beta(1 + \tilde{z})^3]^{-\frac{1}{2}} d\tilde{z}. \quad (\text{A.5})$$

Let us change the integration variable from \tilde{z} to x such that

$$x = (1 + \tilde{z})^3. \quad (\text{A.6})$$

Using this variable, $I(z)$ in Eq. (A.5) becomes

$$I(z) = \frac{\alpha}{3} \int_{\gamma(z=0)}^{\gamma(z)} x^{-\frac{2}{3}} (1 - \beta x)^{-\frac{1}{2}} dx, \quad (\text{A.7})$$

where γ is given as

$$\gamma(z) = (1 + z)^3. \quad (\text{A.8})$$

Eq. (A.7) can be rewritten as

$$I(z) = \frac{\alpha}{3} [\tilde{I}(z) - \tilde{I}(z=0)], \quad (\text{A.9})$$

where \tilde{I} is given as

$$\tilde{I}(z) = \int_0^{\gamma(z)} x^{-\frac{2}{3}} (1 - \beta x)^{-\frac{1}{2}} dx. \quad (\text{A.10})$$

Let us again change the variable from x to y such that

$$y = \frac{x}{\gamma(z)}. \quad (\text{A.11})$$

With the changed variable, Eq. (A.10) can be rewritten as

$$\tilde{I}(z) = (1 + z)f(z), \quad (\text{A.12})$$

$$f(z) = \int_0^1 y^{-\frac{2}{3}} [1 - b(z)y]^{-\frac{1}{2}} dy, \quad (\text{A.13})$$

where we have used the expression of γ from Eq. (A.8). The expression of b is given as

$$b(z) = \beta\gamma(z) = -\frac{\Omega_{\text{m}0}(1 + z)^3}{1 - \Omega_{\text{m}0}}. \quad (\text{A.14})$$

The expression f in Eq. (A.13) can be rewritten as

$$f(z) = \int_0^1 y^{a_2-1} (1-y)^{a_3-a_2-1} [1-b(z)y]^{-a_1} dy, \quad (\text{A.15})$$

$$a_1 = \frac{1}{2}, \quad a_2 = \frac{1}{3}, \quad a_3 = \frac{4}{3}. \quad (\text{A.16})$$

The integration f in Eq. (A.15) is the standard integral form of the hypergeometric function given as

$$\begin{aligned} \int_0^1 y^{a_2-1} (1-y)^{a_3-a_2-1} [1-by]^{-a_1} dy &= \frac{\Gamma(a_2)\Gamma(a_3-a_2)}{\Gamma(a_3)} {}_2F_1(a_1, a_2; a_3; b) \\ &= \frac{\Gamma(a_2)\Gamma(a_3-a_2)}{\Gamma(a_3)} {}_2F_1(a_2, a_1; a_3; b), \end{aligned} \quad (\text{A.17})$$

where Γ stands for the usual Gamma function. Using the integration result of f from Eq. (A.17), using the values of a_1 , a_2 , and a_3 from Eq. (A.16), and using the expression of b from Eq. (A.14), we get the analytical form of \tilde{I} in Eq. (A.12) given as

$$\tilde{I}(z) = 3(1+z) {}_2F_1\left(\frac{1}{3}, \frac{1}{2}; \frac{4}{3}; -\frac{\Omega_{\text{m}0}(1+z)^3}{1-\Omega_{\text{m}0}}\right). \quad (\text{A.18})$$

Using $\tilde{I}(z)$ from Eq. (A.18) in to Eq. (A.9), we get the expression of I given as

$$I(z) = \alpha \left[(1+z) {}_2F_1\left(\frac{1}{3}, \frac{1}{2}; \frac{4}{3}; -\frac{\Omega_{\text{m}0}(1+z)^3}{1-\Omega_{\text{m}0}}\right) - {}_2F_1\left(\frac{1}{3}, \frac{1}{2}; \frac{4}{3}; -\frac{\Omega_{\text{m}0}}{1-\Omega_{\text{m}0}}\right) \right]. \quad (\text{A.19})$$

Finally, using expressions of α from Eq. (A.3) and I from Eq. (A.19) in Eq. (A.1), we get analytical expression of $D_{\text{M} \Lambda\text{CDM}}^{\text{late-time}}$ given as

$$\begin{aligned} D_{\text{M} \Lambda\text{CDM}}^{\text{late-time}}(z) &= \frac{c}{H_0 \sqrt{1-\Omega_{\text{m}0}}} \left[(1+z) {}_2F_1\left(\frac{1}{3}, \frac{1}{2}; \frac{4}{3}; -\frac{\Omega_{\text{m}0}(1+z)^3}{1-\Omega_{\text{m}0}}\right) \right. \\ &\quad \left. - {}_2F_1\left(\frac{1}{3}, \frac{1}{2}; \frac{4}{3}; -\frac{\Omega_{\text{m}0}}{1-\Omega_{\text{m}0}}\right) \right]. \end{aligned} \quad (\text{A.20})$$

Hence the result in Eq. (A.20) is the same as in Eq. (2.3).

B Computation of A and ΔA corresponding to DESI 2024 and other BAO data

Let us define two quantities given as

$$\tilde{D}_M(z) = \frac{D_M(z)}{r_d}, \quad (\text{B.1})$$

$$\tilde{D}_H(z) = \frac{D_H(z)}{r_d}. \quad (\text{B.2})$$

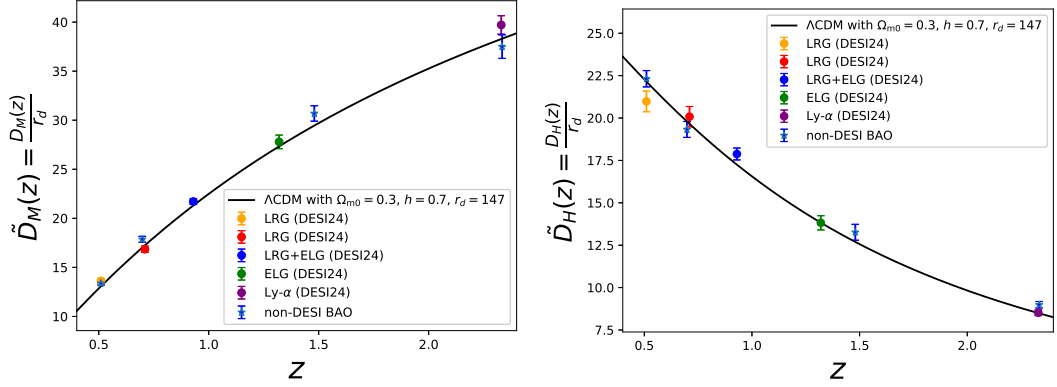


Figure 4. Error bars plots corresponding to \tilde{D}_M , \tilde{D}_H , and the corresponding 1σ errors both for DESI 2024 (denoted by 'DESI24') and other BAO data (denoted by 'non-DESI BAO'). The left panel corresponds to \tilde{D}_M and the associated 1σ errors. The right panel corresponds to \tilde{D}_H and the associated 1σ errors. The continuous black lines correspond to the Λ CDM model with $\Omega_{m0} = 0.3$, $h = 0.7$, and $r_d = 147$.

Sr. No.	tracer (DESI24)	z_{eff}	$\tilde{D}_M \pm \Delta\tilde{D}_M$	$\tilde{D}_H \pm \Delta\tilde{D}_H$	r_{MH}	Refs.
1	LRG	0.51	13.62 ± 0.25	20.98 ± 0.61	-0.445	[63]
2	LRG	0.71	16.85 ± 0.32	20.08 ± 0.60	-0.420	[63]
3	LRG+ELG	0.93	21.71 ± 0.28	17.88 ± 0.35	-0.389	[39]
4	ELG	1.32	27.79 ± 0.69	13.82 ± 0.42	-0.444	[64]
5	Ly- α	2.33	39.71 ± 0.94	8.52 ± 0.17	-0.477	[39]

Table 8. The observed values of \tilde{D}_M , \tilde{D}_H , corresponding 1σ errors, and the correlations between them at five different effective redshifts obtained directly from the DESI 2024 data (denoted as 'DESI24') [39].

These are directly related to the anisotropic BAO observations. We quote the mean and standard deviation values of these two variables in Table 8 corresponding to the DESI 2024 observations.

We have also quoted the correlation between these two variables with a quantity r_{MH} defined as

$$r_{\text{MH}} = \frac{\text{Cov}[\tilde{D}_M, \tilde{D}_H]}{\Delta\tilde{D}_M \Delta\tilde{D}_H}, \quad (\text{B.3})$$

where $\text{Cov}[\tilde{D}_M, \tilde{D}_H]$ denotes the covariances between \tilde{D}_M and \tilde{D}_H . Using the definitions in Eqs. (B.1) and (B.2), the quantity A in Eq. (2.6) (or in Eq. (2.7)) can be rewritten as

$$A = \frac{\tilde{D}_M}{z\tilde{D}_H}. \quad (\text{B.4})$$

The errors (or the standard deviations) in A (denoted as ΔA) can be computed by the propagation of uncertainty given as

Sr. No.	tracer (non-DESI BAO)	z_{eff}	$\tilde{D}_M \pm \Delta\tilde{D}_M$	$\tilde{D}_H \pm \Delta\tilde{D}_H$	r_{MH}	Refs.
1	LRG (BOSS DR12)	0.38	10.234 ± 0.151	24.981 ± 0.582	-0.228	[8]
2	LRG (BOSS DR12)	0.51	13.366 ± 0.179	22.317 ± 0.482	-0.233	[8]
3	LRG (eBOSS DR16)	0.698	17.858 ± 0.302	19.326 ± 0.469	-0.239	[9]
4	QSO (eBOSS DR16)	1.48	30.688 ± 0.789	13.261 ± 0.469	0.039	[70]
5	Ly- α QSO (eBOSS DR16)	2.334	37.5 ± 1.2	8.99 ± 0.19	-0.45	[71]

Table 9. The observed values of \tilde{D}_M , \tilde{D}_H , corresponding 1σ errors, and the correlations between them at five different effective redshifts obtained directly from the other BAO data (denoted as 'non-DESI BAO') [9].

$$\Delta A = \sqrt{\text{Var}[A]}, \quad (\text{B.5})$$

$$\text{Var}[A] = \left(\frac{\partial A}{\partial \tilde{D}_M}\right)^2 \text{Var}[\tilde{D}_M] + \left(\frac{\partial A}{\partial \tilde{D}_H}\right)^2 \text{Var}[\tilde{D}_H] + 2\frac{\partial A}{\partial \tilde{D}_M}\frac{\partial A}{\partial \tilde{D}_H}r_{\text{MH}}\Delta\tilde{D}_M\Delta\tilde{D}_H, \quad (\text{B.6})$$

$$\frac{\partial A}{\partial \tilde{D}_M} = \frac{1}{z\tilde{D}_H}, \quad (\text{B.7})$$

$$\frac{\partial A}{\partial \tilde{D}_H} = -\frac{\tilde{D}_M}{z\tilde{D}_H^2}, \quad (\text{B.8})$$

where $\text{Var}[A]$ means the variance of A . Note that, for simplicity to show the equations, we have omitted the redshift dependence in the equations from Eq. (B.3) to Eq. (B.8). It is understood that the redshift dependence is present in the relevant quantities. Using the above equations and using the values of \tilde{D}_M , \tilde{D}_H and their correlations from Table 8, we compute A and ΔA which are listed in the main text in Table 1.

The values of \tilde{D}_M , \tilde{D}_H and their correlations, obtained from other non-DESI BAO data are listed in Table 9.

To check how close these values of \tilde{D}_M and \tilde{D}_H compared to the reference Λ CDM model, we plot these values in Fig. 4 both for DESI 2024 and other non-DESI BAO data. The left panel corresponds to \tilde{D}_M and the associated 1σ errors. The right panel corresponds to \tilde{D}_H and the associated 1σ errors. The continuous black lines correspond to the Λ CDM model with $\Omega_{\text{m}0} = 0.3$, $h = 0.7$, and $r_d = 147$.

Finally, using the same procedure, we compute A and ΔA for non-DESI BAO observations which are listed in the main text in Table 4.

C Approximate sound horizon at the early time with standard early time physics

The sound horizon r_s is defined as

$$r_s(z) = \int_z^\infty \frac{c_s(\tilde{z})d\tilde{z}}{H(\tilde{z})} = \int_0^{\frac{1}{1+z}} \frac{c_s(a)da}{a^2H(a)}, \quad (\text{C.1})$$

where c_s is the sound speed, a is the cosmic scale factor and it is related to redshift as $a = \frac{1}{1+z}$. For $z \lesssim z_*$, sound speed c_s can be approximated as

$$c_s(a) = \frac{c}{\sqrt{3 \left(1 + \frac{3}{4} \frac{\rho_b(a)}{\rho_\gamma(a)}\right)}} = \frac{c}{\sqrt{3 \left(1 + \frac{3}{4} \frac{\omega_{b0}}{\omega_{\gamma0}} a\right)}}, \quad (\text{C.2})$$

where ρ_b and ρ_γ are the baryon and photon energy densities respectively. In the second equality in Eq. (C.2), $\omega_{\gamma0}$ is defined as

$$\omega_{\gamma0} = \Omega_{\gamma0} h^2, \quad (\text{C.3})$$

where $\Omega_{\gamma0}$ is the photon energy density parameter at present.

The sound speed in Eq. (C.2) can be rewritten as

$$c_s(a) = \frac{c\sqrt{\tilde{\alpha}}}{\sqrt{3}} \frac{1}{\sqrt{a + \tilde{\alpha}}}, \quad (\text{C.4})$$

where $\tilde{\alpha}$ is given as

$$\tilde{\alpha} = \frac{\tilde{\beta}}{\omega_{b0}}. \quad (\text{C.5})$$

In Eq. (C.5), $\tilde{\beta}$ is given as [65, 67]

$$\tilde{\beta} = \frac{4\omega_{\gamma0}}{3} = \frac{\theta^4}{31500}, \quad (\text{C.6})$$

where θ is given as [65, 67]

$$\theta = \frac{T_{\text{CMB}}}{2.7 \text{ Kelvin}}, \quad (\text{C.7})$$

$$T_{\text{CMB}} = 2.7255 \text{ Kelvin}. \quad (\text{C.8})$$

Putting the value of present CMB temperature T_{CMB} from Eq. (C.8) and using Eqs. (C.7) and (C.6), we get approximate value of $\tilde{\beta}$ as

$$\tilde{\beta} \approx 3.29624 \times 10^{-5}. \quad (\text{C.9})$$

By putting Eq. (C.4) in Eq. (C.1) and using the definition $H(z) = H_0 E(z)$, we get an expression for the sound horizon given as

$$r_s(z) = \frac{c\sqrt{\tilde{\alpha}}}{H_0\sqrt{3}} \int_0^{\frac{1}{1+z}} \frac{da}{a^2 E(a) \sqrt{a + \tilde{\alpha}}}. \quad (\text{C.10})$$

In a flat FLRW background, with standard early-time physics, the normalized Hubble parameter can be approximated as

$$E_{\text{standard}}^{\text{early-time}}(z) = \sqrt{\Omega_{m0}(1+z)^3 + \Omega_{r0}(1+z)^4}, \quad (\text{C.11})$$

where Ω_{r0} is the present value of the radiation energy density parameter. Putting Eq. (C.11) in Eq. (C.10) and using the expression in Eq. (3.4), the integral in Eq. (C.10) becomes

$$r_s(z) = \frac{3000\sqrt{\tilde{\alpha}} \text{ Mpc}}{\sqrt{3}\omega_{m0}} \int_0^{\frac{1}{1+z}} \frac{da}{\sqrt{(a + \tilde{\alpha})(a + \tilde{\gamma})}}. \quad (\text{C.12})$$

In Eq. (C.12), $\tilde{\gamma}$ is given as

$$\tilde{\gamma} = \frac{\Omega_{r0}}{\Omega_{m0}} = \frac{1}{1 + z_{\text{eq}}^{\text{m-r}}}, \quad (\text{C.13})$$

where $z_{\text{eq}}^{\text{m-r}}$ is the redshift of radiation and matter equality. It can be written approximately as [65, 67]

$$z_{\text{eq}}^{\text{m-r}} = 25000 \omega_{m0} \theta^{-4} \approx 24077.44059 \omega_{m0}. \quad (\text{C.14})$$

In the last (approximate) equality of Eq. (C.14), we have used Eq. (C.8) and Eq. (C.7). Eq. (C.12) can be rewritten as

$$r_s(z) = \tilde{\delta} \int_0^{\frac{1}{1+z}} \frac{da}{\sqrt{(a + \chi)^2 - \xi^2}}, \quad (\text{C.15})$$

where $\tilde{\delta}$, χ , and ξ are given as

$$\tilde{\delta} = \frac{3000 \sqrt{\tilde{\beta}} \text{ Mpc}}{\sqrt{3\omega_{m0}\omega_{b0}}}, \quad (\text{C.16})$$

$$\chi = \frac{\tilde{\alpha} + \tilde{\gamma}}{2}, \quad (\text{C.17})$$

$$\xi = \frac{\tilde{\alpha} - \tilde{\gamma}}{2}, \quad (\text{C.18})$$

respectively. Now, let us change the integration variable from a to \tilde{a} in Eq. (C.15) such that

$$\tilde{a} = a + \chi, \quad (\text{C.19})$$

and with this changed variable, Eq. (C.15) can be rewritten as

$$r_s(z) = \tilde{\delta} \int_{\chi}^{\frac{1}{1+z} + \chi} \frac{d\tilde{a}}{\sqrt{\tilde{a}^2 - \xi^2}}. \quad (\text{C.20})$$

We now use the integration result given as

$$\int \frac{d\tilde{a}}{\sqrt{\tilde{a}^2 - \xi^2}} = \log \left| \tilde{a} + \sqrt{\tilde{a}^2 - \xi^2} \right| + \text{constant}. \quad (\text{C.21})$$

Note that, here all the variables are positive definite. So, we can neglect the absolute sign in Eq. (C.21). Using this equation and using Eqs. (C.17) and (C.18), we finally get an analytical expression for the approximate sound horizon given as

$$r_s(z) = \tilde{\delta} \log \left[\frac{\frac{1}{1+z} + \frac{\tilde{\alpha} + \tilde{\gamma}}{2} + \sqrt{\tilde{\alpha}\tilde{\gamma} + \frac{\tilde{\alpha} + \tilde{\gamma}}{1+z} + \frac{1}{(1+z)^2}}}{\frac{\tilde{\alpha} + \tilde{\gamma}}{2} + \sqrt{\tilde{\alpha}\tilde{\gamma}}} \right]. \quad (\text{C.22})$$

From Eq. (C.22) and the previous equations, we can see that, for the standard early time physics, the sound horizon depends only on ω_{m0} and ω_{b0} parameters.

D Approximate redshift of photon decoupling with standard early time physics

With the standard early-time physics, the redshift of photon decoupling z_* can be approximated to have an analytical expression given as [65, 67]

$$z_* = 1048 (1 + 0.00124\omega_{\text{b}0}^{-0.738}) (1 + g_1\omega_{\text{m}0}^{g_2}), \quad (\text{D.1})$$

where g_1 and g_2 are given as

$$g_1 = \frac{0.0783\omega_{\text{b}0}^{-0.238}}{1 + 39.5\omega_{\text{b}0}^{0.763}}, \quad (\text{D.2})$$

$$g_2 = \frac{0.560}{1 + 21.1\omega_{\text{b}0}^{1.81}}, \quad (\text{D.3})$$

respectively.

E Brief overview of wCDM, w_0w_a CDM, and z_pw_p CDM parametrizations

The equation of state of dark energy w in the wCDM parametrization, and the Chevallier-Polarski-Linder (CPL) parametrization [34, 35] (w_0w_a CDM parametrization) are given as

$$w(z) = w \quad (\text{wCDM}), \quad (\text{E.1})$$

$$w(z) = w_0 + w_a \frac{z}{1+z} \quad (w_0w_a\text{CDM}), \quad (\text{E.2})$$

respectively. In general, in any dark energy parametrization, the square of the normalized Hubble parameter has the expression (neglecting radiation) given as

$$E^2(z) = \Omega_{\text{m}0}(1+z)^3 + (1 - \Omega_{\text{m}0}) \exp \left[3 \int_0^z \frac{1+w(\tilde{z})}{1+\tilde{z}} d\tilde{z} \right]. \quad (\text{E.3})$$

The z_pw_p CDM parametrization [72, 73] is an alternative parametrization to the w_0w_a CDM parametrization. Here, z_p is the pivot redshift, where the equation of state of dark energy is the most constrained by any data or any combinations of data. At this pivot redshift z_p , the equation of state is denoted by the notation w_p i.e. $w_p \equiv w(z_p)$. To make it equivalent to w_0w_a CDM parametrization, it has the form given as

$$w_p = w_0 + w_a \frac{z_p}{1+z_p}. \quad (\text{E.4})$$

The above equation is derived simply from Eq. (E.2).